

Magnetic Energy Spectra in Solar Active Regions

Valentyna Abramenko and Vasyl Yurchyshyn

Big Bear Solar Observatory, 40386 N. Shore Lane, Big Bear City, CA 92314

ABSTRACT

Line-of-sight magnetograms for 217 active regions (ARs) of different flare rate observed at the solar disk center from January 1997 until December 2006 are utilized to study the turbulence regime and its relationship to the flare productivity. Data from *SOHO*/MDI instrument recorded in the high resolution mode and data from the BBSO magnetograph were used. The turbulence regime was probed via magnetic energy spectra and magnetic dissipation spectra. We found steeper energy spectra for ARs of higher flare productivity. We also report that both the power index, α , of the energy spectrum, $E(k) \sim k^{-\alpha}$, and the total spectral energy $W = \int E(k)dk$ are comparably correlated with the flare index, A , of an active region. The correlations are found to be stronger than that found between the flare index and total unsigned flux. The flare index for an AR can be estimated based on measurements of α and W as $A = 10^b(\alpha W)^c$, with $b = -7.92 \pm 0.58$ and $c = 1.85 \pm 0.13$. We found that the regime of the fully-developed turbulence occurs in decaying ARs and in emerging ARs (at the very early stage of emergence). Well-developed ARs display under-developed turbulence with strong magnetic dissipation at all scales.

Subject headings: Sun: activity - Sun: flares - Sun: photosphere - Sun: surface magnetism - Physical Data and Processes: magnetic fields - Physical Data and Processes: turbulence

1. Introduction

Existing methods to predict flare activity of ARs are not numerous (e.g., Abramenko et al. 2002; Falconer et al. 2002, 2003, 2006; Leka & Barnes 2003, 2007; McAteer et al. 2005; Schrijver 2007; Georgoulis & Rust 2007; Barnes & Leka 2008; see review by McAteer et al. 2009) and majority of them are based on the first-order statistical moments of the magnetic field (test parameters are derived from B). At the same time, Leka & Barnes (2007) noted that exploration of higher order statistical moments seems beneficial given the non-linear nature of a flaring process.

Earlier we presented results of a small statistical study (Abramenko 2005) focused on the relationship between flare productivity of solar active regions (ARs) and the power-law index, α , of magnetic energy spectrum, $E(k) \sim k^{-\alpha}$. This magnetic energy spectrum technique is based on the second-order statistical moment of a 2D field, and it shows distribution of energy over spatial scales. The study was based on 16 ARs observed predominantly during 2000 - 2003 with the *SOHO*/MDI instrument (Scherrer et al. 1995) performing in the high resolution (HR) mode. The findings were promising: flaring ARs were reported to display steeper power spectra with the power index exceeding the magnitude of 2. Flare-quiet ARs exhibited a Kolmogorov-type spectrum with α close to 5/3 (Kolmogorov 1991, referred hereinafter K41).

Power spectra calculations, based on the technique described in Abramenko (2005) will be a part of the pipeline system designed to process real-time data flowing from Helioseismic and Magnetic Imager¹ that operates on board of the *Solar Dynamics Observatory*². Here we evaluate performance of the method based on a large data set. We report that both the magnetic energy stored in large-scale structures and the magnetic energy cascaded by turbulence at small-scale structures (below 10 Mm), are comparably correlated with flare productivity (Section 3). From the magnetic energy spectra we also determined at what spatial scales the bulk of the magnetic energy dissipation occurs (Section 4). This allowed us to make an inference about the characteristics of the turbulent regime in ARs, which may be useful as a constraint criterion for the MHD modeling of ARs.

2. Data

We selected 217 active regions measured near at the solar disk center (no further than 20 degrees away from the central meridian), so that the projection effect can be neglected. The set covers the period between January 1997 and December 2006. All the ARs displayed nonzero flare activity, i.e., at least one GOES flare flare was produced by an AR during its passage across the solar disk. Given typical average flux densities in active regions, smooth power spectra are not usually obtained for active regions with unsigned magnetic flux less than 10^{22} Mx. Therefore, we required that each AR should possess unsigned magnetic flux that exceeds this threshold value.

For majority of ARs (215), MDI/HR magnetograms (pixel size of $0.6''$) were utilized.

¹<http://hmi.stanford.edu/>

²<http://sdo.gsfc.nasa.gov/>

For two extremely flare-productive ARs only Big Bear Solar Observatory (BBSO) data, obtained at very good seeing conditions with the Digital Magnetograph (DMG, Spirock 2005, pixel size of $0.6''$) were available. As we have shown earlier (Abramenko et al. 2001) magnetic energy spectra calculated for the same AR from MDI/HR and BBSO/DMG magnetograms agree very well at scales larger than 3 Mm. This allows us to use different data without risk of skewing the correlation. From MDI full disk magnetograms we determined the trend in the total unsigned flux in each AR during a 3-day time interval centered at the time of MDI/HR magnetogram acquisition. When AR flux variations did not exceed $\pm 10\%$ of the mean value we classified the AR as a stable, well-developed AR. ARs displaying larger monotonous changes of the flux were classified as emerging or decaying. Unipolar sunspots were detected by visual assessment.

Flare productivity of an AR was measured by the flare index, A , introduced in Abramenko (2005). Since the X-ray classification of solar flares (X, M, C, and B) is based on denary logarithmic scale, we can define the flare index as

$$A = (100S^{(X)} + 10S^{(M)} + S^{(C)} + 0.1S^{(B)})/t. \quad (1)$$

Here, $S^{(j)}$ is the sum of all GOES flare magnitudes in the j -th X-ray class:

$$S^{(j)} = \sum_{i=1}^{N_j} I_i^{(j)}, \quad (2)$$

where $N_j = N_X, N_M, N_C$ and N_B are the numbers of flares of X, M, C and B classes, respectively, that occurred in a given active region during its passage across the solar disk that is represented by the time interval t measured in days. $I_i^{(j)} = I_i^{(X)}, I_i^{(M)}, I_i^{(C)}$ and $I_i^{(B)}$ are GOES magnitudes of X, M, C and B flares. The interval t was taken to be 27/2 days for the majority of the ARs with exception of emerging ones. In general, those ARs that produced only C-class flares have flare indices smaller than 2, whereas several X-class flares will result in the flare index exceeding 100. The highest flare index of 584 was registered for NOAA AR 10486 which, unfortunately, was not included in the analysis because it was outside of the MDI/HR field of view.

3. Magnetic Energy Spectra

Photospheric plasma is thought to be in a turbulent state, subject to the continuous sub-photospheric convection. It can be analyzed with the energy spectrum (which is frequently referred as a power spectrum). The energy spectrum is based on the second-order statistical moments of a field and it is very useful to probe the inter-scale energy cascade and dissipation regimes (see, e.g., Monin & Yaglom 1975; Biskamp 1993).

Our method to calculate the 1D angle-integrated energy spectrum, $E(k)$, of a 2D structure (e.g., a line-of-sight magnetogram, $B_z(x, y)$) was described in Abramenko et al. (2001) and later improved in Abramenko (2005). The most reliable scale interval to derive the energy cascade in the spectrum is 3 - 10 Mm when utilizing MDI/HR and BBSO data (Abramenko et al., 2001). At scales smaller than 2-3 Mm, the influence of insufficient resolution is substantial, while the contribution from large sunspots at scales exceeding 10 Mm contaminates the slope of the turbulent cascade in the spectrum. For all the ARs, we used the above linear interval to measure the power index, α , of the magnetic energy spectrum, $E(k) \sim k^{-\alpha}$, where k is a wave number inversely proportional to the spatial scale, $r = 2\pi/k$. The index was computed from the best linear fit in the double logarithmic plot via the IDL/LINFIT routine by minimizing the χ -square error statistic. Figure 1 shows energy spectra for three ARs of different flare productivity which is evident from different steepness of the slopes. The well-defined power-law energy cascade interval is observed at 3-10 Mm in all cases.

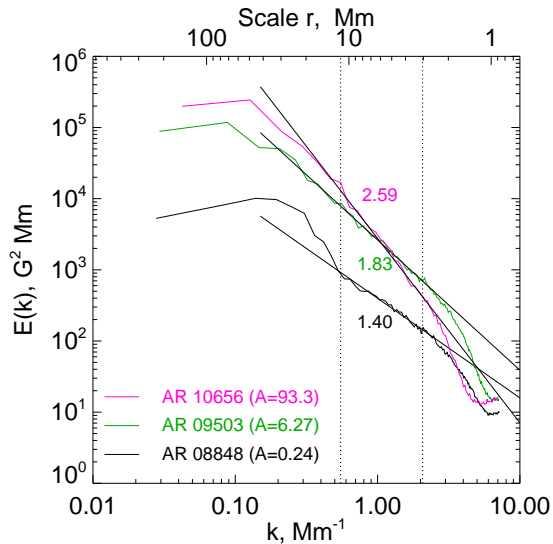


Fig. 1.— Magnetic energy spectra, $E(k)$, shown for three ARs with different flare index, A . Vertical dotted segments mark the linear interval between 3-10 Mm, where the the best linear fits (thin lines) were calculated. The power index, α , defined as $E(k) \sim k^{-\alpha}$ and measured as a slope of the best fit for each spectrum is shown.

The relationship between the power and flare indexes is shown in Figure 2a. Positive correlation between these parameters ($\rho = 0.57$ with the 95% confidence interval of 0.478

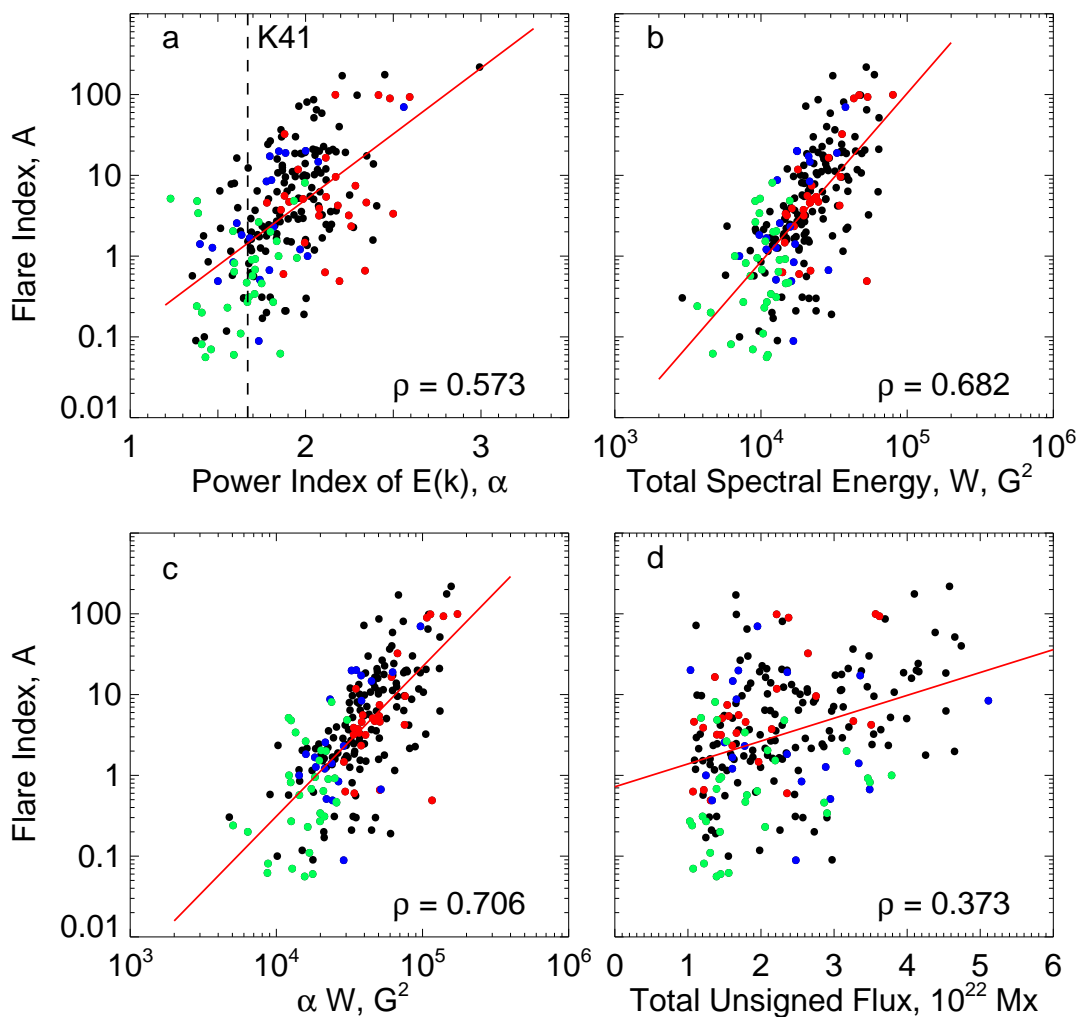


Fig. 2.— The flare index, A plotted versus: *a* - the power index, α , of the magnetic energy spectrum (the vertical dashed segment marks the power index of the fully-developed Kolmogorov-type turbulence of $\alpha = 5/3$); *b* - the total spectral energy, W ; *c* - the power index weighted by the total spectral energy, W ; *d* - the total unsigned flux. The solid lines show the best linear fits to the data points. The correlation coefficients, ρ , are shown. Black, red, blue and green circles mark well-developed, emerging, decaying ARs and unipolar sunspots, respectively.

- 0.66 according to the Fisher's Z-transformation statistical test of significance³) allows

³<http://icp.giss.nasa.gov/education/statistics/page3.html>

us to conclude that, in general, steeper spectra are associated with higher flaring rate. Unipolar active regions (green circles) form a separate low-flaring/shallow-spectrum subset. Emerging, decaying and stable ARs are distributed more or less uniformly over the diagram.

Comparison of the spectra in Figure 1 also suggests that not only the slope, but the amplitudes of a spectrum may be related to flare productivity. Thus, we calculated two additional parameters from the spectra. The first parameter, $\langle E(k_{low}) \rangle$, characterizes the amplitude of a spectrum at low wave numbers and is derived as $E(k)$ averaged over the interval ranging from the smallest k to $k = 2\pi/10 \text{ Mm}^{-1}$. The correlation coefficient between this parameter and the flare index A is 0.65 with the 95% confidence interval of 0.57 - 0.72. The second parameter is the total spectral energy, $W = \int E(k)dk$, where the integration is performed over all wavenumbers where the $E(k)$ is non-zero. On average, $85 \pm 5 \%$ of the total spectral energy is concentrated at scales larger than 10 Mm, so that W may be considered as a measure of energy accumulated in large-scale structures of an AR. The correlation between W and the flare index A (see Figure 2 *b*) was found to be somewhat higher: $\rho = 0.68$ with the 95% confidence interval of 0.60 - 0.75.

Note that, W can also be computed directly from B_z^2 according to Parseval's theorem (e.g., Kammler 2000). However, computing W via integration of a Fourier transform has an advantage because the integration over an annulus also acts as a noise filter by leaving out high-frequency corners in the 2D wave number box. When analyzed data come from MDI/HR, the difference in derived values is less than 0.5%. However, the difference increases when ground-based data are analyzed. When a mixed data set is used (space and ground bases observations), the values of W derived via integration of the Fourier transform are more consistent. Therefore, the total spectral energy used here was calculated using the integration approach.

So, the power index of the spectrum, the total spectral energy and the averaged large-scale amplitude are comparably correlated with the flare index. We may conclude that both the turbulent energy cascade and the presence of large-scale structures in an AR are relevant to flare activity.

For the purpose of prediction of AR's flare productivity, we weighted the total spectral energy, W , and the power index, α , to capture the contribution of both small-scale and large-scale effects (Figure 2*c*). The correlation coefficient in this case increased to 0.71 with the 95% confidence interval of 0.63 - 0.77. The flare index can be then fitted assuming

$$A = 10^b(\alpha W)^c, \tag{3}$$

where $b = -7.92 \pm 0.58$ and $c = 1.85 \pm 0.13$, with the reduced $\chi^2 = 0.29$.

In general, the most powerful flares occur in strong, large ARs with considerable

amount of the magnetic flux (e.g., Barnes & Leka 2008). And yet, the total unsigned flux is only very weakly correlated to the flare index (Figure 2*d*, the correlation coefficient is 0.37 with the 95% confidence interval of 0.25 - 0.49). This is understandable when we recall previous studies showing that not only the magnetic flux but rather *complexity* of the magnetic structure is relevant to the flaring rate (Sammis et al. 2000; Abramenko et al. 2002; Falconer et al. 2002, 2003, 2006; Leka & Barnes 2003, 2007; McAteer et al. 2005; Schrijver 2007; Georgoulis & Rust 2007).

4. Magnetic Dissipation Spectra

As it follows from Figure 2*a*, the majority of ARs (especially those of high flare activity) display energy spectra steeper than the Kolmogorov-type spectrum. To infer a physical meaning of this result, we will analyze the magnetic energy dissipation rates and magnetic dissipation spectra.

Magnetic energy dissipation rate is related to the presence of electric currents, i.e., $\langle \varepsilon \rangle \sim \eta \langle \mathbf{j}^2 \rangle$ (e.g., Biskamp 1993). In MHD models of turbulence, dissipative structures are visualized via (squared) currents (e.g., Biskamp & Welter 1989; Biskamp 1996; Schaffenberger et al. 2006; Pietarila Graham et al. 2009; Servidio et al. 2009) which appear in 2D images to be predominantly located along magnetic field discontinuities frequently referred to as current sheets. From 2D MHD modeling, Biskamp and Welter (1989) found that when the magnetic Reynolds number (which is the ratio of characteristic values of advection terms to the magnetic diffusivity and quantifies the strength of advection relative to magnetic diffusion) is low, these current sheets are extended and rare, and they become shorter and more numerous as Reynolds number increases. Thus, the magnetic dissipation spectrum represents the distribution of dissipative structures over many spatial scales, and it is a reasonable proxy for statistics of current structures in an AR.

The magnetic dissipation spectrum allows us probe the state of turbulence. For fully developed turbulence (K41, high Reynolds number), the bulk of magnetic energy dissipation occurs at small scales, k_d , whereas the the energy input occurs at large scales, k_e , (Figure 3) and energy cascades from large to small scales without losses. When the energy input interval and the dissipation interval overlap, dissipation occurs at intermediate scales, along the cascade. This condition occurs in the state of under-developed turbulence (low Reynolds number), when large-scale structures might interfere with the turbulent cascade at small scales. It is a challenge to model such a field because no K41 simplifications are applicable.

The magnetic energy dissipation spectra are defined as (Monin & Yaglom 1975,

Biskamp 1993):

$$E_{dis}(k) = 2\eta k^2 E(k), \quad (4)$$

where η is the magnetic diffusivity coefficient. (Note that E and E_{dis} in Eq. 4 have different dimensions.) Then the rate of magnetic energy dissipation normalized by the magnetic diffusivity can be derived as (Biskamp 1993):

$$\langle \varepsilon \rangle / \eta = 2 \int_0^\infty k^2 E(k) dk. \quad (5)$$

From observations we can derive function $k^2 E(k)$, which is proportional to the dissipation spectrum under an assumption that η is uniform over the AR area. In our case both $k^2 E(k)$ and $\langle \varepsilon \rangle / \eta$ are associated with dissipation of the B_z component only.

We calculated $k^2 E(k)$ spectra for all ARs in our data set. Typical examples are shown in Figure 4. At the early stage of development of emerging ARs, the separation distance ($k_d - k_e$) is largest, which is similar to the fully-developed turbulence conditions seen in quiet Sun (see Figure 3). Later on this distance decreases as k_d shifts toward smaller wavenumbers (larger scales), so that the intervals of energy and dissipation become exceedingly overlapping. This implies formation of large-scale dissipative structures. Decaying magnetic complexes show quite opposite behavior (Figure 4, middle row). Well-developed ARs (bottom row in Figure 4) show a significant overlap of the energy and dissipation intervals suggesting that, to the contrary of the fully developed turbulence phenomenology, significant dissipation takes place at all spatial scales. Thus, for the majority of well-developed ARs, one should expect a state of under-developed turbulence in the photosphere with the dissipation of the magnetic energy at all observable spatial scales.

We then compared the magnitudes of $\langle \varepsilon \rangle / \eta$ to the flare index, A . Their correlation turned out to be positive with $\rho = 0.53$ with the 95% confidence interval of 0.43 - 0.62. This indicates that the rate on magnetic energy dissipation in the photosphere is relevant to flare activity.

5. Conclusions and Discussion

In this study we analyzed second-order statistical moments of solar magnetic fields of 217 active regions observed with the MDI instrument in high resolution mode during the 23rd solar cycle.

The angle-integrated magnetic energy spectra of solar ARs display a well-defined power-law region, which indicates the presence of a turbulent non-linear energy cascade.

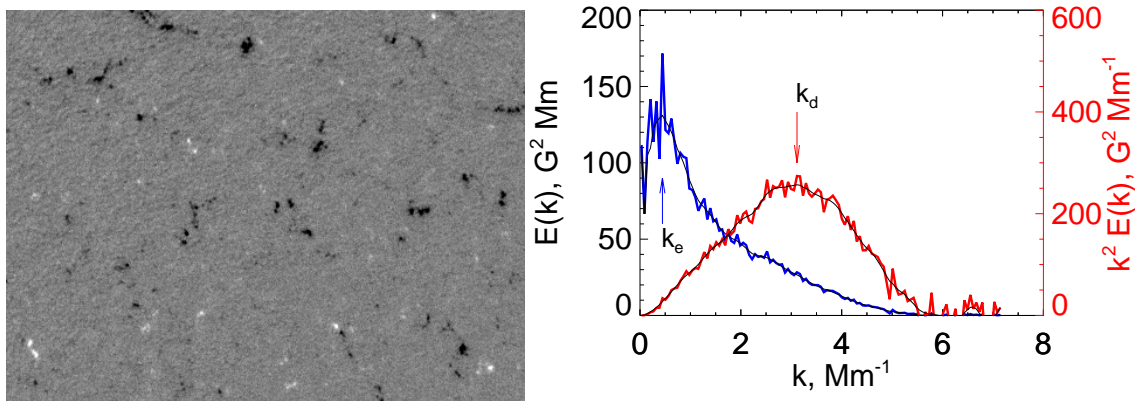


Fig. 3.— MDI/HR magnetogram for a quiet sun area recorded on 2001 June 5/13:07 UT (*left*) and corresponding spectra (*right*): the energy spectrum $E(k)$ (*blue curve and right axis*) and dissipation spectrum, $k^2 E(k)$ (*red curve, left axis*). The image size is 266×202 arcsec. The magnetogram is scaled from -150 G to 150 G. The arrows k_e and k_d mark the maxima of the energy (k_e) and dissipation (k_d) spectra. Positions of the maxima were derived by 5 point box car averaging (*black curves*). The maxima of the energy and dissipation spectra are distinctly separated in the wavenumber space.

The power index, α measured at 3-10 Mm scale range was found to be well correlated with the flare index, A (correlation coefficient, $\rho = 0.57$). This results further supports our previous findings based on only 16 ARs (Abramenko 2005). The power indices range between 1.3 and 3.0, with the majority of ARs having the power index in the range of 1.6 – 2.3. No particular preference for the classical 5/3 index was found. These values are in a surprising agreement with recent numerical simulations of decaying MHD turbulence (Lee et al. 2009). The model results showed that in equivalent initial magnetic configurations different types of spectra (from $k^{-3/2}$ to k^{-2}) may emerge depending on the intrinsic non-linear dynamics of the flow.

The total spectral energy, $W = \int E(k)dk$, is found to be well correlated with the flare index ($\rho = 0.68$), while spectral energy weighted by the power index shows the strongest correlation to the flare index ($\rho = 0.71$), which allowed us to determine an empirical description of this relationship: $A = 10^b(\alpha W)^c$, where $b = -7.92 \pm 0.58$ and $C = 1.85 \pm 0.13$.

Combined analysis of magnetic energy and magnetic dissipation spectra showed that in majority of well-developed ARs, the turbulent energy cascade is augmented by magnetic energy dissipation at all scales. We thus argue that a state of under-developed turbulence exists in the photosphere of mature ARs.

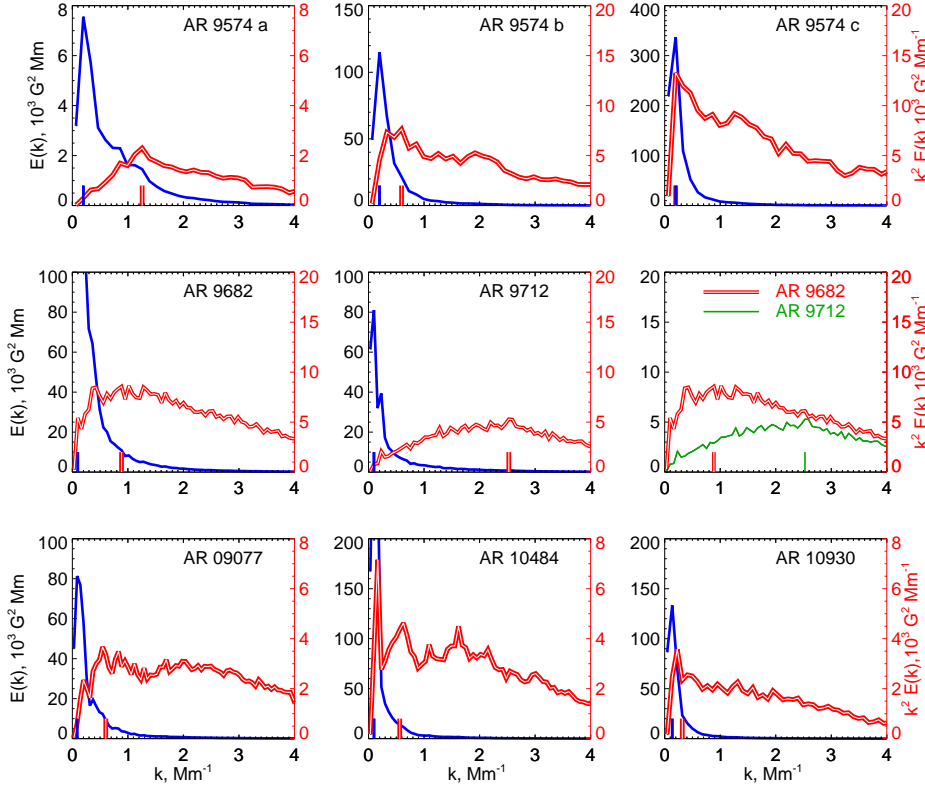


Fig. 4.— *Top* - energy spectra, $E(k)$ (blue lines), and dissipation spectra, $k^2 E(k)$ (double red lines), plotted for an emerging AR. Panels *a*, *b* and *c* correspond to three consecutive moments during the emergence. Vertical blue (red) bars mark the maximum of the energy (dissipation) spectrum. Blue bars correspond to k_e and red bars correspond to k_d . As the active region emerges, k_d shifts toward the smaller wavenumbers. *Middle* - energy and dissipation spectra for a decaying magnetic complex NOAA ARs 9682 and 9712. The right panel shows a superposition of the dissipation spectra at the well-developed (double red line) and decaying (solid green line) state of the magnetic complex. As the magnetic fields decay, k_d shifts toward small scales (larger wavenumbers). *Bottom* - energy spectra and dissipation spectra for three well-developed ARs. The spectra are overlapped for each case.

The magnetic energy dissipation rate, $\langle \varepsilon \rangle / \eta$, correlates with the flare productivity in the same degree as the power index does ($\rho = 0.53$). As long as energy dissipation rate is proportional to electric currents squared, we argue that the presence of currents is relevant

to flare productivity. Also, good correlation between the energy dissipation rate and the flaring rate is in agreement with earlier reports by Schrijver et al. (2005).

It is known from direct calculations based on vector-magnetograms that electric currents are ubiquitous in ARs (see, e.g., Abramenko et al. 1991; Leka et al. 1993, 1996; Pevtsov et al. 1994; Abramenko et al. 1996; Wheatland 2000; Zhang 2002; Schrijver et al. 2005; Leka & Barnes 2007; Schrijver et al. 2008; Schrijver 2009). We found here that photospheric magnetic fields are in a state of under-developed turbulence when both the energy cascade and energy dissipation at all scales are present in the system. We therefore, arrive at a conclusion that both large and small scale dissipative structures (currents) are relevant to flaring.

On the other hand, Fisher et al. (1998) found no correlation between photospheric currents and soft X-ray luminosity of ARs. This was also noted, but not discussed, by Schrijver et al. (2005). We suggest that this apparent controversy is due to different nature of flares and the soft X-ray emission. We may consider flares as sporadic explosive events caused by strongly non-linear dynamics relevant to large- and small-scale magnetic discontinuities (Falconer et al. 2002, 2003, 2006, see also Schrijver 2009), whereas soft X-ray emission reflects a more stationary and homogeneous process of coronal heating rather related to ubiquitous small scale discontinuities formed *in-situ* (Klimchuk 2006).

We would also like to note that the power law of the magnetic energy spectra, explored in this paper, shall not be confused with the power law found in the distribution of the magnetic flux in flux concentrations reported recently by Parnell et al. (2009). At first sight, both of them characterize the *structure* of the magnetic field. However, they address different physical consequences of the magnetic field structuring. The power law of the magnetic energy spectrum represents distribution of magnetic energy, B^2 , over spatial scales and quantifies turbulence in an AR. Here, the smallest magnetic elements are represented by the tail of the spectrum usually associated with low spectrum amplitudes. The power law found in distribution of magnetic flux represents frequency (abundance) of magnetic elements of different sizes and implies a unique mechanism of formation of magnetic flux concentrations (say, fragmentation process, see Abramenko & Longcope (2005) for more discussion). The smallest magnetic elements are the most frequent and they are represented by the highest amplitudes of the distribution.

Modern computational capabilities allow us to develop MHD models which take into account turbulent regime and turbulent dissipation (e.g., Lionello et al. 2010; Klimchuk et al. 2010). Therefore, diagnostics of turbulence derived from a large uniform data set is essential for constructing and restraining of these models.

We are grateful to anonymous referee for criticism and useful comments allowing to improve substantially the manuscript. SOHO is a project of international cooperation between ESA and NASA. This work was supported by NSF grant ATM-0716512 and NASA grants NNX08AJ20G and NNX08AQ89G.

REFERENCES

- Abramenko, V. I., Gopasiuk, S. I., Ogir', M. B. 1991, *Solar Phys.*, 134, 287
- Abramenko, V. 2005, *ApJ*, 629, 1141
- Abramenko, V. I., Wang, Tongjiang, Yurchishin, V. B. 1996, *Solar Phys.*, 168, 75
- Abramenko, V., Yurchyshyn, V., Wang, H. & Goode, P. R. 2001, *Sol. Phys.*, 201, 225
- Abramenko, V.I., Yurchyshyn, V.B., Wang, H., Spirock, T.J., Goode, P. R., 2002, *ApJ*, 577, 487
- Abramenko, V. I., Longcope, D. W. 2005, *ApJ*, 619, 1160 , the correlation coefficient is 0.37
- Barnes, G., Leka, K. D. 2008, *ApJ*, 688, L107
- Biskamp, D. 1993, *Nonlinear Magnetohydrodynamics* (Cambridge University Press, New York)
- Biskamp, D. 1996, *Astrophys. and Space Sci.* 242, 165
- Biskamp, D., Welter, H. 1989, *Phys. Fluids*, B1, 1964
- Falconer, D.A., Moore, R.L., Gary, G.A., 2002, *ApJ*, 569, 1016
- Falconer, D.A., Moore, R.L., Gary, G.A., 2003, *JGR*, 108, 1380
- Falconer, D.A., Moore, R.L., Gary, G.A., 2006, *ApJ*, 644, 1258
- Fisher, George H.; Longcope, Dana W.; Metcalf, Thomas R.; Pevtsov, Alexei A. 1998, *ApJ*, 508, 885
- Georgoulis, M. K. & Rust, D. M. 2007, *ApJL*, 661, L109
- Kammler, D.W. 2000, *A First Course in Fourier Analysis* (Prentice-Hall, Inc., Upper Saddle River, NJ) p. 74.
- Klimchuk, J. 2006, *Solar Phys.*, 234, 41

- Klimchuk, J. A., Nigro, G., Dahlburg, R. B., Antiochos, S. K. 2010, American Astronomical Society, AAS Meeting #216, Abstract #302.05
- Kolmogorov, A.N. 1991, Proceedings of the Royal Society of London. Series A: Mathematical and Physical Science, 434, 9.
- Lee, E., Brachet, M.E., Pouquet, A., Mininni, P.D., Resenberg, D. 2009, arXiv:0906.2506v1
- Leka, K. D., Canfield, R. C., McClymont, A. N., de La Beaujardiere, J.-F., Fan, Y., & Tang, F. 1993, ApJ, 411, 370
- Leka, K. D., Canfield, R. C., McClymont, A. N., & van Driel-Gesztelyi, L. 1996, ApJ, 462, 547
- Leka, K. D. & Barnes, G. 2003, ApJ, 595, 1277
- Leka, K. D. & Barnes, G. 2007, ApJ, 656, 1173
- Lionello, Roberto, Linker, J. A., Mikic, Z., Riley, P., Velli, M. 2010, American Astronomical Society, AAS Meeting #216, Abstract #303.01
- McAteer, R.T., Gallagher, P.T., Ireland, J. 2005, Astrophys. J., 631, 628.
- McAteer, R.T.J., Gallagher, P.T., Conlon, P.A. 2009, Adv. in Space Res., 45, Issue 9, 1067
- Monin, A.S. & Yaglom, A.M. 1975, Statistical Fluid Mechanics, ed. J.Lumley (MIT Press, Cambridge, MA)
- Parnell, C. E., DeForest, C. E., Hagenaar, H. J., Johnston, B. A., Lamb, D. A., Welsch, B. T. 2009, ApJ, 698, 75
- Pevtsov, A.A., Canfield, R.C., Metcalf, T.R. 1994, ApJL, 425, L117
- Pietarila Graham, J., Mininni, P. D., Pouquet, A. 2009, Physical Review E, 80, 016313
- Sammis, I, Tang, F, Zirin, H. 2000, Astrophys. J, 540, 583
- Schaffnerberger, W., Wedemeyer-Bhm, S., Steiner, O., Freytag, B. 2006, in: Solar MHD Theory and Observations: A High Spatial Resolution Perspective ASP Conference Series, Vol. 354, Edited by J. Leibacher, R. F. Stein, and H. Uitenbroek. San Francisco: Astronomical Society of the Pacific, 345
- Schrijver, C. J., De Rosa, M.L., Title, A. M., Metcalf, T. R. 2005, ApJ, 628, 501
- Schrijver, C. J. 2007, ApJL, 655, L117

- Schrijver, C. J.; De Rosa, M. L.; Metcalf, T. and 14 co-authors 2008, *ApJ*, 675, 1637.
- Schrijver, C. J. 2009, *Adv. in Space Res.*, 43, 739
- Scherrer, P.H., Bogart, R.S., Bush, R.I., Hoeksema, J.T., Kosovichev, A.G., Schou, J., Rosenberg, W., Springer, L., Tarbell, T.D., Title, A., Wolfson, C.J., Zayer, I. and the MDI engineering team, 1995, *Sol. Phys.*, 162,129
- Servidio, S., Matthaeus, W. H., Shay, M. A., Cassak, P. A., Dmitruk, P. 2009, *Phys. Rev. Let.*, 102, 115003
- Spirock, T.J. 2005, PhD thesis, New Jersey Institute of Technology.
- Wheatland, M. S. 2000, *ApJ*, 532, 616
- Zhang, H. 2002, *Mon. Not. R. Astron. Soc.*, 332, 500